A device adaptive inflow boundary condition for Wigner equations of quantum transport

Haiyan Jiang [a], Tiao Lu [b], Wei Cai [c]

[a] *Department of Applied Mathematics, Beijing Institute of Technology, Beijing 100081,China*

[b] *HEDPS & CAPT, LMAM and School of Mathematical Sciences, Peking University, Beijing 100871, China.*

[c] *Department of Mathematics and Statistics, University of North Carolina at Charlotte, Charlotte, NC 28223-0001*

Suggested Running Head:
A device adaptive inflow boundary condition for Wigner equations

Corresponding Author:
Prof. Wei Cai
Department of Mathematics and Statistics,
University of North Carolina at Charlotte,
Charlotte, NC 28223-0001
Phone: 704-687-4581, Fax: 704-687-6415,
Email: wcai@uncc.edu
H.J. and T.L. contributed equally to this work.

AMS Subject classifications: 65M06, 81S30, 81Q99, 82C10, 35S15

Abstract

In this paper, an improved inflow boundary condition is proposed for Wigner equations in simulating a resonant tunneling diode (RTD), which takes into consideration the band structure of the device. The original Frensley inflow boundary condition prescribes the Wigner distribution function at the device boundary to be the semi-classical Fermi-Dirac distribution for free electrons in the device contacts without considering the effect of the quantum interaction inside the quantum device. The proposed device adaptive inflow boundary condition includes this effect by assigning the Wigner distribution to the value obtained from the Wigner transform of wave functions inside the device at zero external bias voltage, thus including the dominant effect on the electron distribution in the contacts due to the device internal band energy profile. Numerical results on computing the electron density inside the RTD under various incident waves and non-zero bias conditions show much improvement by the new boundary condition over the traditional Frensley inflow boundary condition.

Key words: Frensley inflow boundary condition, Wigner function, Resonant tunneling diode.

1. Introduction

As semiconductor devices are being scaled down to nanometer dimensions, the quantum effects, such as size quantization and tunneling, become important in studying the properties of the devices [1] [2]. The non-equilibrium Green function (NEGF) formalism and the Wigner equation are two popular simulation methods in quantum transport of nano-scale devices as open systems. For ballistic transport, the NEGF formalism is equivalent to solving the Schrödinger equation [3] [4] while it also introduces self-energy for treating device contacts attached to the active device region [5], and a phenomenal treatment of the bodily scattering effects [6,7]. On the other hand, the Wigner distribution, defined via a Wigner-Weyl transform of the density correlation function of the quantum device, is introduced by E. Wigner in 1932 as an analog of the classical Boltzmann distribution for the quantum system [8]. Being a quantum kinetic analog of the classical Boltzmann equation, the Wigner equation has advantages over the NEGF method in two aspects [9,10]. One is that the Wigner framework allows the modeling of scattering phenomena for the quantum kinetic equation. The other is that its phase space formulation makes it easier to impose boundary conditions for the Wigner distribution at the device contacts, using the knowledge of the semi-classical distribution such as the Fermi-Dirac distribution for electrons in the device contacts [11].

In the last decades, the Wigner equation has received much attention in simulating quantum transport of nano-scale devices [11–13]. It was originally used for studying the current-voltage characteristics of RTDs by Frensley [11]. Frensley successfully reproduced the negative differential resistance by using an upwind finite difference method for the Wigner equation with an inflow boundary condition. This work motivated later work on Wigner based numerical simulations of nano-scale devices [14,13,15–22]. Furthermore, self-consistent Wigner-Poisson equations were used in [23] [24] to clarify the origin of the hysteresis and a plateau-like structure of the I-V curve of RTDs. Recent works on the comparison between the Wigner equation and the NEGF for double gate MOSFETs [22] [4] and for RTDs [17] [18] have produced qualitatively similar results. However, these results also show that the transport current calculated by the Wigner equation method with the Frensley inflow boundary condition is higher than that by the NEGF method [4]. Recently, Jiang *et al.* investigated how the accuracy of the inflow boundary condition is affected by the size of contact regions included in the simulation domain of the RTD [25]. In [25], it was found that the Frensley inflow boundary condition for incoming electrons holds exactly only infinite away from the active device region and its accuracy depends on the length of the contacts included in the simulation. This result implies that, in order to get more accurate results, larger regions of the contacts should be included, which would lead to higher computational cost. Therefore, it is necessary to design a better inflow boundary condition for

smaller contact region to reduce the computational cost while still preserving numerical accuracy.

The Frensley inflow boundary condition specifies the distribution function at the contacts to be some given function, most often in practice, the Fermi-Dirac distribution. Electrons entering the device will interact with the intrinsic band structure of the active device region, resulting in reflection and transmission electrons into the incoming and opposite sides of the device, respectively. For RTDs, electrons tunnel through the band structure profile through resonant coupling, in addition to interacting with other electrons through quantum interference and collisions. These quantum effects will influence the Wigner distribution function at the boundary as the Wigner function by definition is constructed through a global Wigner transform of the density correlation function [8]. In Frensley's original paper [11], the band structure profile inside the device is totally ignored when setting the boundary condition. In this paper, we will propose a device adaptive boundary condition which reflects the dominant effect of the device internal band structure in prescribing the values of the Wigner distributions at the device boundaries. In general, the electron wave functions inside a quantum device for non-zero bias will be hard to predict a prior. Therefore, our strategy will only consider the dominant quantum interaction inside the device, namely, the states of the electrons inside the device at zero bias under the impact of incident free electron, so called scattering states of the electrons [26,27]. We will then compute the corresponding Wigner distribution of these scattering states and the resulting distributions will be used as the boundary data for the Wigner distribution function for general non-zero bias situations. This new boundary condition will be called the device adaptive boundary condition (DABC) as the internal band structure is indirectly used in the prescription of the Wigner distribution in the contacts. We expect, as validated by our numerical tests, the new DABC will improve the density profile inside the device for a reasonably wide range of applied external bias.

The rest of the paper is organized as follows. The Wigner function and its truncated version and their governing equations are introduced in Section 2. Section 3 gives the original Frensley inflow boundary condition and then the improved device adaptive inflow boundary condition. A upwind finite difference method to the Wigner equation is described in Section 4 and the numerical studies of the DABC are presented in Section 5. Finally, Section 6 gives the conclusion of the paper and discussion on future work.

2. Wigner fucntion and its truncated version using the correlation length L_{coh}

In this paper, the stationary and linear Wigner equation will be used for finding better inflow boundary condition for the Wigner distribution functions. The Wigner equation is a quantum kinetic equation derived from the Schrödinger equation as a quantum mechanical analogue to the Boltzmann equation [8,28]. In the following the key idea of the derivation of the Wigner equation for pure states is sketched.

The stationary Schrödinger equation for an electron of the effective mass m in a potential energy $V(x)$ reads

$$-\frac{\hbar^2}{2m}\frac{\partial^2\psi(x)}{\partial x^2} + V(x)\psi(x) = E\psi(x), \tag{1}$$

where $\psi(x)$ is the eigen wavefunction and E is the eigen energy. If the state of a quantum system can be described completely with a given wave function $\psi(x)$, we will consider the quantum system in a pure state. Otherwise, if the quantum system can be found in states described in multiple wave functions in specific probability, then we consider the quantum system in a mixed state. The density matrix $\rho(x, x')$ for a pure state system is defined simply as

$$\rho(x, x') = \psi(x)\psi^*(x'), \tag{2}$$

which satisfies the von Neumann equation

$$-\frac{\hbar^2}{2m}\left[\frac{\partial^2}{\partial x^2} - \frac{\partial^2}{\partial x'^2}\right]\rho(x, x') + [V(x) - V(x')]\,\rho(x, x') = 0. \tag{3}$$

The von Neumann equation (3) is equivalent to the Schrödinger equation (1) in the sense that either can be derived from the other, but the former holds advantage over the latter in describing quantum systems in mixed states [29].

The Wigner function is defined through the Wigner-Weyl transform of the density matrix $\rho(x, x')$, i.e.

$$f(x, q) = \frac{1}{2\pi}\int_{-\infty}^{+\infty} \rho\left(x + \frac{r}{2}, x - \frac{r}{2}\right)\exp(-\mathrm{i}qr)dr. \tag{4}$$

Based on this definition, the electron density is related to the Wigner function by

$$\rho(x) \equiv \rho(x, x) = \int_{-\infty}^{+\infty} f(x, q)dq. \tag{5}$$

The Wigner-Weyl transform of the von Neumann equation (3) yields the following Wigner equation

$$\frac{q\hbar}{m}\frac{\partial f(x,q)}{\partial x}+\Theta(V)(f)=0, \tag{6}$$

where

$$\Theta(V)(f)=\int_{-\infty}^{+\infty}V_w(x,q-q')f(x,q')dq' \tag{7}$$

and the Wigner potential $V_w(x,q)$ is

$$V_w(x,q)=\frac{\mathrm{i}}{2\pi\hbar}\int_{-\infty}^{+\infty}\left[V\left(x+\frac{r}{2}\right)-V\left(x-\frac{r}{2}\right)\right]\exp(-\mathrm{i}qr)dr. \tag{8}$$

2.1 Truncated Wigner function $f(x,q;L_{\mathrm{coh}})$

For many quantum systems, it can be assumed that the correlation of the density matrix at two locations x and x' will decay to zero as the distance between them goes to infinity, i.e.,

$$\lim_{|x-x'|\to\infty}\rho(x,x')=0. \tag{9}$$

So the Wigner distribution function $f(x,q)$ defined in (4) can be approximated by a truncated Wigner function

$$f(x,q;L_{\mathrm{coh}})=\int_{-\infty}^{\infty}\rho\left(x+\frac{r}{2},x-\frac{r}{2}\right)\chi_{B(0,L_{\mathrm{coh}}/2)}(r)\exp(-\mathrm{i}qr)dr, \tag{10}$$

where L_{coh} is the truncation length beyond which the correlation of the density matrix is ignored, $B(0,L_{\mathrm{coh}}/2)=(-L_{\mathrm{coh}}/2,L_{\mathrm{coh}}/2)$, and the characteristic function is

$$\chi_{B(0,L_{\mathrm{coh}}/2)}(r)=\begin{cases}1, \text{ if } |x|<L_{\mathrm{coh}}/2,\\ 0, \text{ otherwise.}\end{cases} \tag{11}$$

Obviously, as L_{coh} goes to infinity, the truncated Wigner function defined in (10) converges to the Wigner function defined in (4), i.e.,

$$\lim_{L_{\mathrm{coh}}\to\infty}f(x,q;L_{\mathrm{coh}})=f(x,q). \tag{12}$$

Multiplying $\chi_{B(0,L_{\mathrm{coh}})}(x-x')$ on both sides of the von Neumann equation (3), and applying the Wigner-Weyl transform, we obtain a truncated Wigner equation

$$\frac{q\hbar}{m}\frac{\partial f(x,q;L_{\mathrm{coh}})}{\partial x}+\Theta(V)(f(x,q;L_{\mathrm{coh}}))=0, \tag{13}$$

where

$$\Theta(V)(f(x,q;L_{\rm coh})) = \frac{\mathrm{i}}{2\pi\hbar}\int_{-\infty}^{\infty}[V(x+r/2)-V(x-r/2)] \\ \chi_{B(0,L_{\rm coh})}(r)\rho(x+r/2,x-r/2)\exp(-\mathrm{i}qr)dr. \tag{14}$$

Using the convolution theorem of the Fourier transform and the obvious identity

$$\chi_{B(0,L_{\rm coh})}(r) = \left(\chi_{B(0,L_{\rm coh})}(r)\right)^2,$$

we have

$$\Theta(V)(f(x,q;L_{\rm coh})) = \int_{-\infty}^{\infty} V_w(x,q-q';L_{\rm coh})f(x,q';L_{\rm coh})dq', \tag{15}$$

where

$$V_w(x,q;L_{\rm coh}) = \frac{\mathrm{i}}{2\pi\hbar}\int_{-\infty}^{\infty}[V(x+r/2)-V(x-r/2)]\,\chi_{B(0,L_{\rm coh})/2}(r)\exp(-\mathrm{i}qr)dr, \tag{16}$$

namely,

$$\begin{aligned} V_w(x,q;L_{\rm coh}) &= \frac{\mathrm{i}}{2\pi\hbar}\int_{-L_{\rm coh}/2}^{L_{\rm coh}/2}[V(x+r/2)-V(x-r/2)]\exp(-\mathrm{i}qr)dr \\ &= \frac{1}{\pi\hbar}\int_{0}^{L_{\rm coh}/2}\sin(qr)\left[V\left(x+\frac{r}{2}\right)-V\left(x-\frac{r}{2}\right)\right]dr. \end{aligned} \tag{17}$$

If we use $\Theta(V)(f(x,q))$ to denote the nonlocal Wigner potential term in (6),

$$\Theta(V)(f) = \int_{-\infty}^{+\infty} V_w(x,q-q')f(x,q')dq', \tag{18}$$

it is clear that by using (10) and (16) we have

$$\Theta(V)(f(x,q;L_{\rm coh})) \to \Theta(V)(f(x,q)), \quad \text{as } L_{\rm coh}\to\infty. \tag{19}$$

Thus, the truncation length $L_{\rm coh}$ will determine the accuracy of (13) compared with the original Wigner equation (6) and can be increased for better accuracy.

3. Device adaptive boundary condition (DABC)

3.1 Frensley inflow boundary condition

The Frensley inflow boundary condition is of the Dirichlet type in the phase space and specifies the incoming flow, as determined by the sign of the wave

number q in (13), on the left and right contacts. Here the electrons in the contacts are considered free electrons modeled by a unit plane wave according to (1) with $V(x) = 0$,

$$\psi(x) = \exp(\mathrm{i}kx), \tag{20}$$

where k is the wave number and is related to the energy level E of the electron in a dispersion relation as follows

$$E = \frac{\hbar^2 k^2}{2m}. \tag{21}$$

According to the definition of the Wigner function (4), the Wigner function for free electrons is then

$$f^{\mathrm{in}}(x,q) = \int_{-\infty}^{+\infty} \psi\left(x + \frac{r}{2}\right) \psi^*\left(x - \frac{r}{2}\right) \exp(-\mathrm{i}qr)dr = \delta(k-q). \tag{22}$$

Therefore, $\delta(k-q)$ will be used as the inflow boundary condition if the device is impacted with a unit incident wave. Most previous simulation work using the Wigner equation for nano-devices (MOSFETs, RTDs) adopted this boundary condition. From (22), the boundary condition of the Wigner equation with unit injection from the left ($k > 0$) is then

$$f(0,q) = \ \delta(q-k),\ q > 0, \quad \text{and} \quad f(L,q) = 0,\ q < 0. \tag{23}$$

For numerical simulations, the Dirac delta function in the boundary condition above is approximated by a discrete version of the delta function

$$f(0,q) = \begin{cases} \frac{1}{h_q}, \text{ if } q = k, \\ 0, \quad \text{if } q \neq k \text{ and } q > 0, \end{cases} \tag{24}$$

where h_q is the mesh size in the q-space.

3.2 Device structure and boundary condition

The quantum interaction occurring inside a quantum device will unavoidably change the electron behavior inside the contacts, especially when the length of the contacts for the simulation is selected to be as small as possible for computational cost concern. The free electron assumption in the Frensley boundary condition in (20) and (24) does not consider such an influence of the device on the contact electrons. Recent studies have shown the boundary condition and the contact lengths can greatly affect the accuracy of the simulation with the Wigner equation for resonant tunneling diodes [4]. In the following we will present a new boundary value for the Wigner equation for better accuracy

by including the quantum interaction from the device itself in the case of a typical RTD structure shown in Fig. 1.

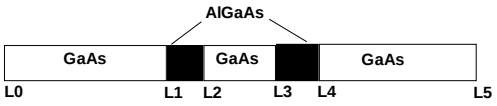

Fig. 1. The structure of a typical resonant tunneling diode

The RTD is a classical 1-D hetero-structure device with a negative resistance, which is composed of two thin AlGaAs layers sandwiched between GaAs layers to form two energy barriers and one quantum well. If we consider a varying effective mass in the RTD, then the 1-D Schrödinger equation is

$$-\frac{\hbar^2}{2}\frac{\partial}{\partial x}\left(\frac{1}{m(x)}\frac{\partial}{\partial x}\right)\psi(x) + V(x)\psi(x) = E\psi(x), \tag{25}$$

where the effective mass of GaAs is $m_{GaAs} = 0.067m_0$ and that of AlGaAs is $m_{AlGaAs} = 0.0919m_0$, and m_0 is the rest electron mass. In this paper, we will not consider the position dependence of the effective mass and instead use a constant effective mass $m_x = m_{GaAs} = 0.067m_0$. The prototype of RTDs is a symmetric structure, and we denote $L_{ij} = L_j - L_i$. The black barrier region is set to $L_{21} = L_{43} = 2.825$nm, the length of the quantum well is $L_{32} = 4.52$nm, and the length of the left/right contact region is $L_{10} = L_{54} = 17.515$nm.

The ideal potential energy profile of the band structure for the RTD is illustrated in Fig. 2. And the potential energy function is

$$V(x) = \begin{cases} 0, & L_0 < x < L_1, \\ E_g, & L_1 \le x \le L_2, \\ 0, & L_2 < x < L_3, \\ E_g, & L_3 \le x \le < L_4, \\ 0, & L_4 < x < L_5, \end{cases} \tag{26}$$

where $E_g = 0.27$eV is the conduction band offset between GaAs and AlGaAs.

Assuming that a free electron is injected with energy E from the left contact of the device at zero bias (equilibrium state), then, we can solve the wave

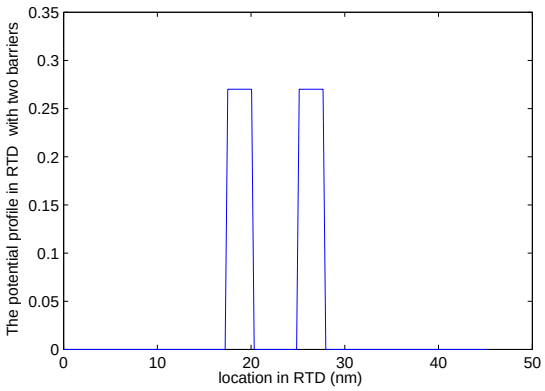

Fig. 2. The potential energy $V(x)$ at the equilibrium state

function $\psi_e(x)$ for the equilibrium state analytically as follows

$$\psi_e(x) = \begin{cases} \exp(\mathrm{i}k_1 x) + b_0 \exp(-\mathrm{i}k_1 x), & L_0 < x < L_1, \\ b_1 \exp(\mathrm{i}k_2 x) + b_2 \exp(-\mathrm{i}k_2 x), & L_1 \le x \le L_2, \\ b_3 \exp(\mathrm{i}k_1 x) + b_4 \exp(-\mathrm{i}k_1 x), & L_2 < x < L_3, \\ b_5 \exp(\mathrm{i}k_2 x) + b_6 \exp(-\mathrm{i}k_2 x), & L_3 \le x \le L_4, \\ b_7 \exp(\mathrm{i}k_1 x), & L_4 < x < L_5, \end{cases} \tag{27}$$

where $k_1 = \sqrt{\dfrac{2mE}{\hbar^2}}, k_2 = \sqrt{\dfrac{2m(E-E_g)}{\hbar^2}}$. $b_i, i = 0, 1, 3, ..., 7$ can be obtained by solving an 8×8 complex linear system according to the continuity of the wave function and flux at L_1, L_2, L_3, and L_4

$$\psi_e(L_i - 0) = \psi_e(L_i + 0), \qquad \frac{\partial \psi_e(L_i - 0)}{\partial x} = \frac{\partial \psi_e(L_i + 0)}{\partial x}, \quad i = 1, 2, 3, 4.$$

The truncated Wigner function for the equilibrium state is

$$f^e(x, q; L_{\mathrm{coh}}) = \int_{-\infty}^{+\infty} \psi_e \left(x + \frac{r}{2}\right) \psi_e^* \left(x - \frac{r}{2}\right) \chi_{B(0, L_{\mathrm{coh}}/2)}(r) \exp(-\mathrm{i}qr) dr. \tag{28}$$

The equilibrium Wigner function $f^e(x, q; L_{\mathrm{coh}})$ now contains the quantum interaction in the presence of the internal structure of the device, and this function will be used to provide the boundary data for the Wigner function for general non-zero bias Wigner functions as follows.

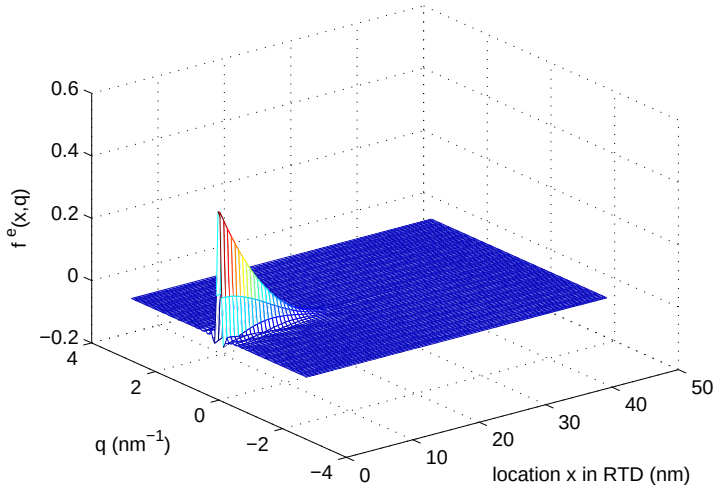

Fig. 3. The truncated Wigner function $f^e(x, q; L_{\text{coh}})$ for a unit wave injected with $k_1 = \dfrac{h_q}{2}$ from the left side

- **Device adaptive boundary condition (DABC)**

$$f(0, q; L_{\text{coh}}) = f^e(0, q; L_{\text{coh}}), \text{ for } q > 0, \text{ and } f(L, q; L_{\text{coh}}) = 0, \text{ for } q < 0. \tag{29}$$

Remark 1 *For the non-equilibrium state, a better boundary value for the Wigner distribution should be found by the Wigner function associated with the wave functions for the device under the corresponding bias, which is in general not available. Therefore,the boundary value given in (29) for the non-equilibrium non-zero bias case is only approximate. However, our numerical tests will show that even for that case, the boundary condition (29) will still improve the electron density calculation significantly over the traditional Frensley boundary condition (24).*

4. A finite difference method for the Wigner equation

For simplicity, we will denote the truncated Wigner function $f(x, q; L_{\text{coh}})$ as $f(x, q)$ and the Wigner potential $V_w(x, q; L_{\text{coh}})$ as $V_w(x, q)$. An upwind finite difference method will be used to solve (13), (15) and (17) as proposed in [25] where details concerning on the numerical implementation, such as the numerical conservation and the relation between L_{coh} (the correlation length) and h_q (the mesh size in the wave vector space), are discussed.

As we will only need to compute the Wigner function $f(x,q)$ for $|q| < \frac{L_q}{2}$ for some large value L_q, we will zero-out the distribution function $f(x,q) = 0$ if $|q| > \frac{L_q}{2}$. Thus (15) becomes

$$\Theta(V)(f(x,q)) = \int_{-L_q/2}^{L_q/2} V_w(x, q-q')f(x,q')dq'. \tag{30}$$

Plugging (30) into (13) yields

$$\frac{\hbar q}{m_x}\frac{\partial}{\partial x}f(x,q) + \int_{-L_q/2}^{L_q/2} V_w(x, q-q')f(x,q')dq' = 0, \tag{31}$$

which will be solved in the (x,q) space by a finite difference scheme. We set h_x be the mesh size of the x-space, and N be the number of the mesh points,

$$h_x = \frac{L}{N}, \quad x_i = -\frac{L}{2} + ih_x, \quad i = 0, 1, 2, ..., N. \tag{32}$$

From (31), only the boundary condition in the x-space is required. An upwind finite difference method is used to approximate the first order derivative in x. The infinite integration with respect to q and r should be truncated to finite ranges. Let $[0, \frac{L_{\rm coh}}{2}]$ be the integration domain in (17) and $N_{\rm coh}$ denote the number of the mesh points with a spacing $h_{\rm coh} = \frac{L_{\rm coh}}{N_{\rm coh}}$. Similarly, we let L_q be the integration length in (31), which will be selected by the mass conservation requirement (36). N_q is the number of the mesh points with a spacing $h_q = \frac{L_q}{N_q}$. In order to avoid $q = 0$ which would lead to a zero element in the diagonal of the discretization matrix for the derivative operator, we choose the mesh points as $q_j = \frac{L_q}{2} - \left(j + \frac{1}{2}\right) h_q, \quad j = 0, 1, 2, \cdots, N_q - 1$.

Using a middle point formula for the integration with respect to q' in (31) and the first order upwind finite difference scheme for the spatial derivative, we arrive at a finite difference equation at (x_i, q_j)

$$\begin{array}{l} \frac{\hbar q_j}{m_x}\frac{f(x_i,q_j) - f(x_{i-1},q_j)}{h_x} + h_q \sum_{j'=0}^{N_q-1} V_w(x_i, q_j - q'_{j'})f(x_i, q'_{j'}) = 0, \; q_j > 0, \\ \frac{\hbar q_j}{m_x}\frac{f(x_{i+1},q_j) - f(x_i,q_j)}{h_x} + h_q \sum_{j'=0}^{N_q-1} V_w(x_i, q_j - q'_{j'})f(x_i, q'_{j'}) = 0, \; q_j < 0, \end{array} \tag{33}$$

for $i = 1, 2, 3, \cdots, N-1$, and $j = 0, 1, 2, \cdots, N_q - 1$. Here, $V_w(x_i, q_j - q'_{j'})$ is calculated by a numerical integration on a uniform mesh of spacing $h_{\rm coh}$, say, $h_{\rm coh} = 2h_x$.

With a trapezoidal rule, we have (note that we only need to evaluate $V_w(x,q)$

at multiples of h_q)

$$V_w(x_i, jh_q) = \frac{h_{\text{coh}}}{\pi\hbar} \sum_{k=1}^{N_{\text{coh}}/2-1} \sin(kh_{\text{coh}}jh_q) \left[V(x_{i+k}) - V(x_{i-k})\right], \tag{34}$$

for integers $j = -N_q + 1, -N_q + 2, \cdots, N_q - 1$. As the continuous Fourier transform is changed to the discrete Fourier transform, to use the fast discrete Fourier transform in (34) we require

$$kh_{\text{coh}}jh_q = kj\frac{L_{\text{coh}}h_q}{N_{\text{coh}}} \Rightarrow L_{\text{coh}}h_q = 2\pi. \tag{35}$$

To ensure the mass conservation, L_q must satisfy [11]

$$L_q h_{\text{coh}} = 2\pi. \tag{36}$$

Observing (35) and (36), one can find that the values of L_q and L_{coh} are related by

$$\frac{L_q}{h_q} = \frac{L_{\text{coh}}}{h_{\text{coh}}}, \tag{37}$$

which implies that

$$N_q = N_{\text{coh}}.$$

5. Numerical results

As the DABC in (29) includes the dominant quantum interaction inside the device active region, we expect the Wigner equation with the new boundary condition will perform better than the traditional Frensley inflow boundary condition. We will conduct a series of numerical tests to show the improved performance in computing the electron density $\rho(x)$ throughout the RTD under various bias conditions and with various contact lengths. We denote the Frensley inflow boundary condition by "Frensley BC" and the device adaptive inflow boundary condition (29) by "device adaptive BC" or simply DABC. In all the calculations for the truncated Wigner function $f^e(x, q; L_{\text{coh}})$ in (28), L_{coh} is taken to be twice the length of the RTD device under study.

The reference solutions for the density profile inside the RTDs are calculated by the NEGF method for the single energy incident electron cases (Tests one to three) as the NEGF together with a Sommerfeld radiation condition is shown [4] to be equivalent to solving the Schrodinger equation directly. It was shown previously [25] that the Wigner equation with the Frensley BC on a sufficiently long contact will agree with the NEGF method and, therefore,

the former method is used to compute the reference solution in Test four in accessing the performance of the DABC for multi-energy incident electrons. In all cases, the potential energy profile $V(x)$ inside the RTD at non-zero bias voltage is assumed to be a piecewise linear extension of the case given in (26) for zero bias.

- Test One: Single energy incident electron

In the first test, we consider a unit electron wave $\exp(ik_1x), k_1 = \dfrac{h_q}{2}$ injected into the RTD with the contact length $L_c = 17.515$nm under different bias voltages. Fig. 4 presents the absolute error of the density. Obviously, the DABC gives a more accurate density distribution compared with the Frensley inflow boundary condition. The same conclusion can be arrived at Figs. 5 and 6. The wave number of the unite wave $\exp(ik_1x)$ is increased to $k_1 = \dfrac{3h_q}{2}$ in Fig. 5. The case with the wave function $\exp(-\mathrm{i}k_1x), k_1 = \dfrac{h_q}{2}$ injected from the right contact is shown in Fig. 6. All three cases clearly show a remarkable improvement of the electron density obtained by using the DABC over that obtained by using the traditional Frensley inflow boundary condition.

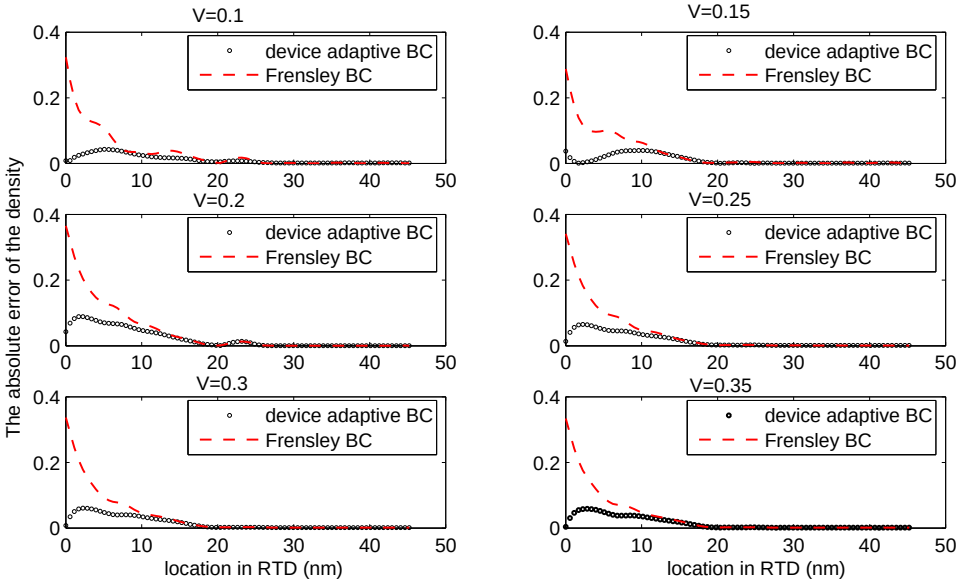

Fig. 4. The absolute error of the density for an injected wave with $k_1 = \dfrac{h_q}{2}$

- Test Two: Effect of device internal structure

In this test, we will show that the improvement of the electron density by using DABC in (29) for the Wigner equation comes from its use of the correct

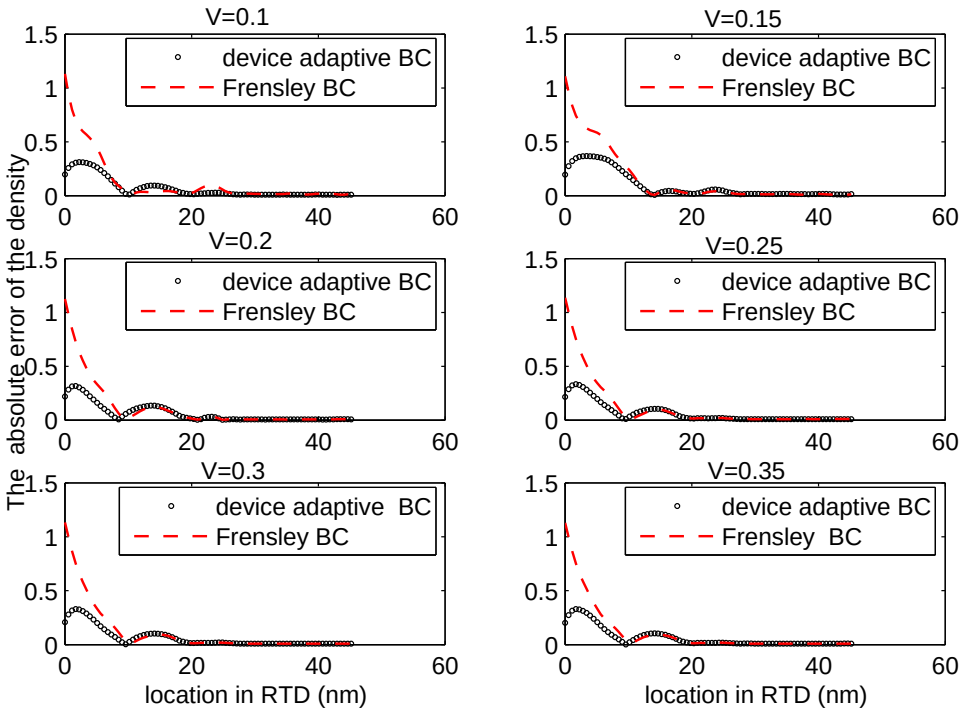

Fig. 5. The absolute error of the density for an injected wave with $k_1 = \dfrac{3h_q}{2}$

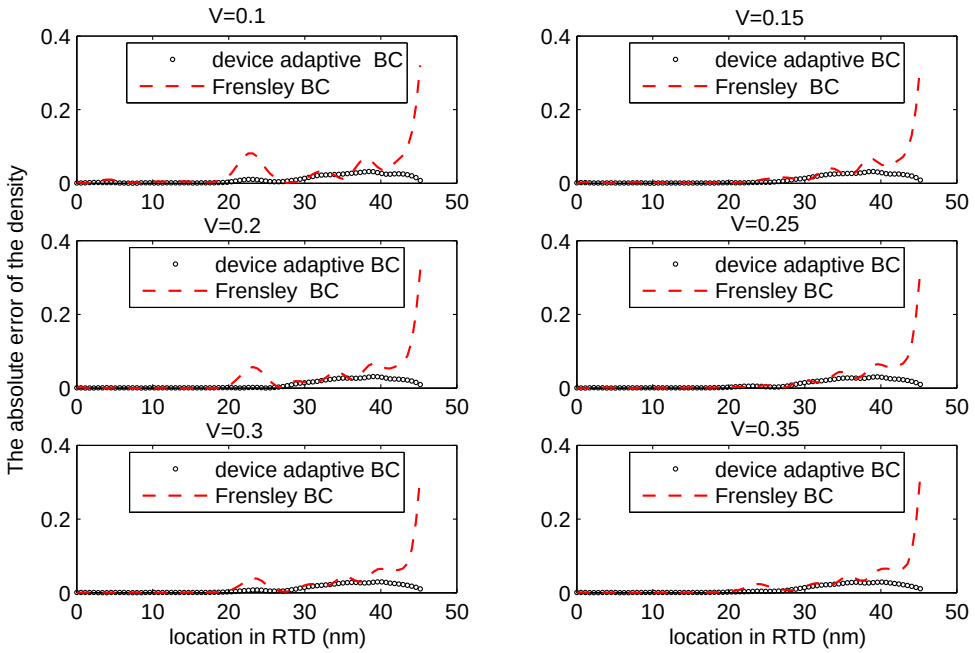

Fig. 6. The absolute error of the density for an injected wave with $k_1 = -\dfrac{h_q}{2}$

characteristics of the quantum devices in assigning the boundary value for the Wigner function in the contacts. For example, the double barrier structures and the single barrier structure will behave differently when impacted by incident electron waves as indicated by their different transmission coefficients. Fig. 8 presents how the transmission coefficient T_{sd} changes with the wave number q in three cases. The figure shows different transmission characteristics for the three cases, indicating different quantum interactions for each case. One salient feature for the double barrier structure is that it allows resonant tunneling (a main characteristic of RTDs) while a single barrier structure does not.

In order to show that it is important to use the correct property of the double barrier structure in RTD devices for designing a good DABC, we first compute the numerical solutions of a RTD device by using the DABC based on a single barrier structure. We use the left or right barrier in the double barrier structure to represent the main effect of the RTD device as in Fig. 7. The absolute errors of the density calculated by the Wigner equation are depicted in Fig. 9. The result using the DABC based on the right barrier is worse than that using the original Frensley inflow boundary condition, and of course, both are worse than the result using the DABC based on the double barrier structure. However, the result using the DABC based on the left single barrier structure is close to the result using the DABC based on the double barrier structure. The reason for this is that the reflection wave due to the left single barrier alone is close to that due to the double barriers for incident waves at low energies. However, the reflection from only the right barrier in the double barrier structure will have a phase error, and the resulting Wigner function in (28) will be quite different from those obtained by considering the double barrier reflection. These differences can be clearly seen in Figs. 10 and 11 for the Wigner function $f^e(x, q; L_{\text{coh}})$ in (28) based on the wave functions for the three cases at zero bias. Especially, Fig. 11 shows the difference between the boundary data used in (29) of DABC and in (24) for the original Frensley BC.

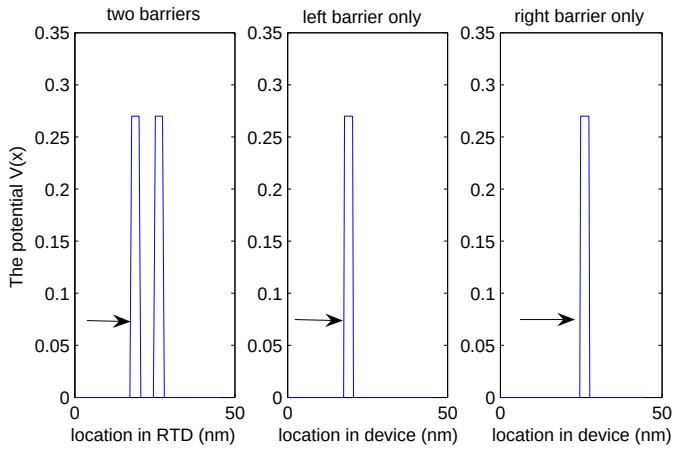

Fig. 7. The structure of the two-barrier and one-barrier devices

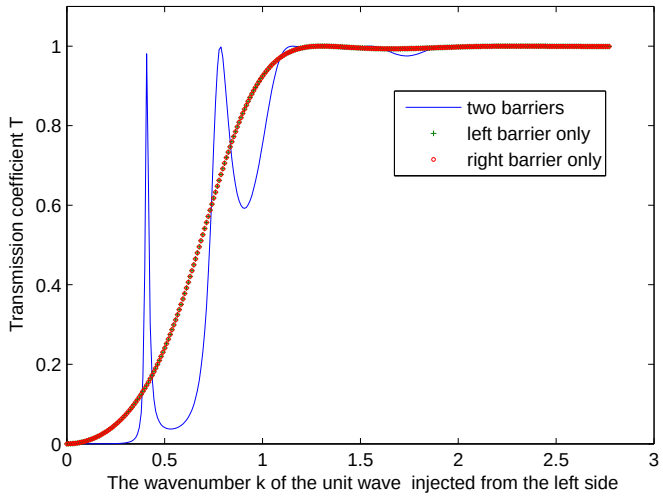

Fig. 8. The transmission coefficient T_{sd} vs the wave number q of unit injection from the left

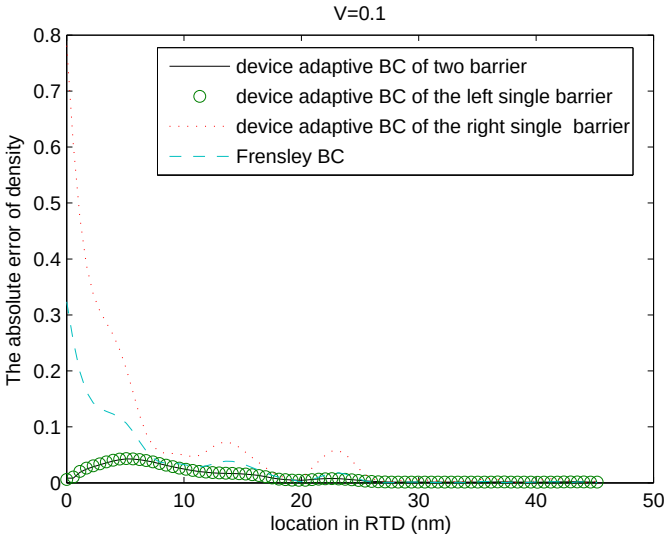

Fig. 9. The absolute error of the density for an injected wave with $k_1 = \dfrac{h_q}{2}$

- Test Three: Effect of contact length

Next, we would like to investigate the effect of the contact length and the accuracy obtained by both the Frensley boundary condition and the DABC. From the distribution function (28) used in the definition of the DABC (29), it can be seen that for a fixed correlation length L_{coh}, as the length of the contact becomes long enough, the DABC is equivalent to the Frensley boundary condition. It has been shown in [25] that as the length of the contact used with the Frensley inflow boundary condition increases, the numerical result becomes more accurate. This point is shown in Fig. 12 by comparing the absolute errors of the density $\rho(x)$ calculated by using the Frensley inflow boundary

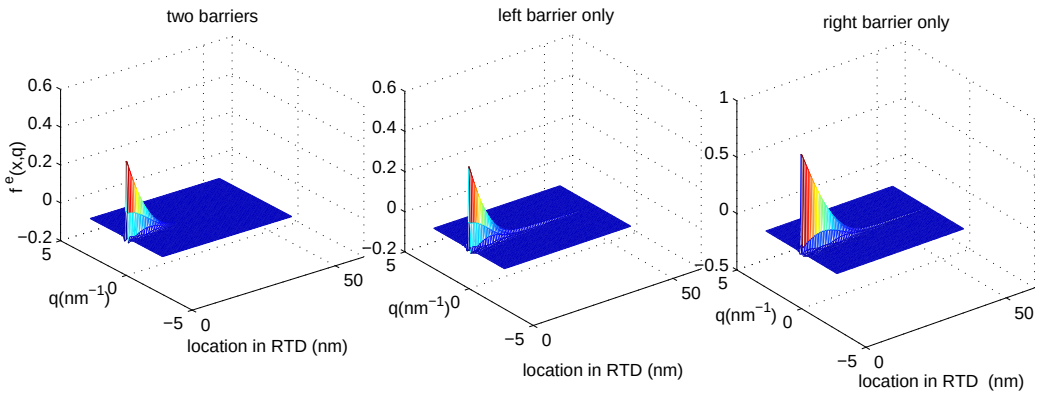

Fig. 10. The truncated Wigner function $f^e(x,q)$ for a unit wave injected with $k_1 = \dfrac{h_q}{2}$ from the left side

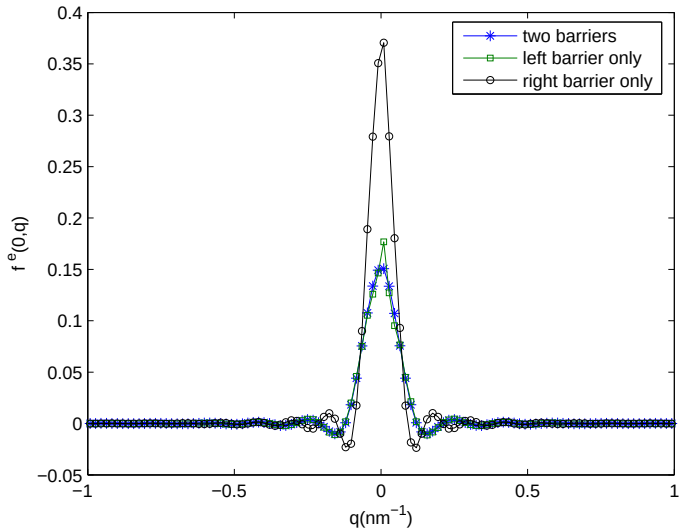

Fig. 11. The truncated Wigner function $f^e(0,q)$ for a unit wave injected with $k_1 = \dfrac{h_q}{2}$ from the left side

condition with the contact length $L_c = 20a, 30a, 40a, 50a$ ($a = 0.565$nm is the lattice constant of GaAs). The result for the DABC in Fig. 13 shows that for a shorter contact length $L_c = 20a$ the DABC yields an error similar to that using the Frensley inflow boundary condition with much longer contact length $L_c = 50a$. Fig. 13 also shows that the DABC is not as sensitive to the contact length as the Frensley inflow boundary condition. Finally, Fig. 14 demonstrates that for a given accuracy, twice contact lengths are needed for the Frensley inflow boundary condition compared with those needed for the

DABC.

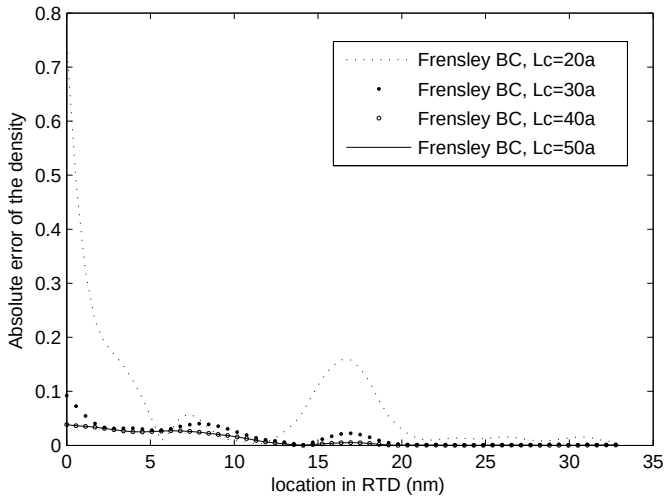

Fig. 12. The absolute error of the density with the Frensley inflow boundary condition

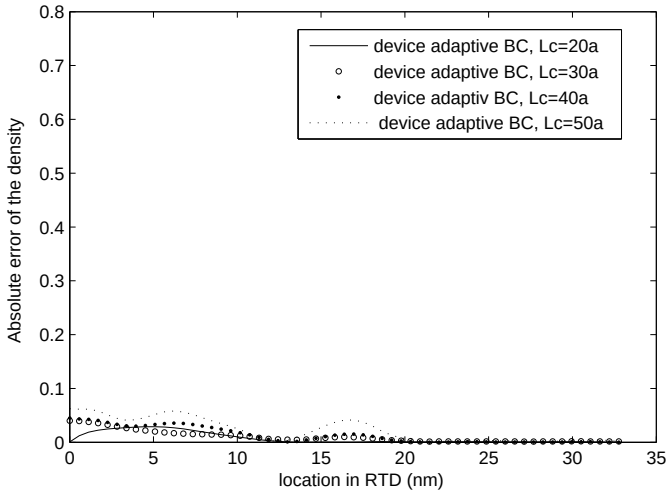

Fig. 13. The absolute error of the density with the improved inflow boundary condition

• Test Four: Incident electrons with multiple energy levels

Finally, we compare the results using the DABC and the Frensley inflow boundary condition in Fig. 15 when multi-energy electron injections from both sides are considered. The density obtained using the DABC with $L_c = 20a$ is plotted in the left sub-figure, comparing with that of the Frensley boundary condition with $L_c = 20a$ and $L_c = 40a$, respectively. It shows the density of

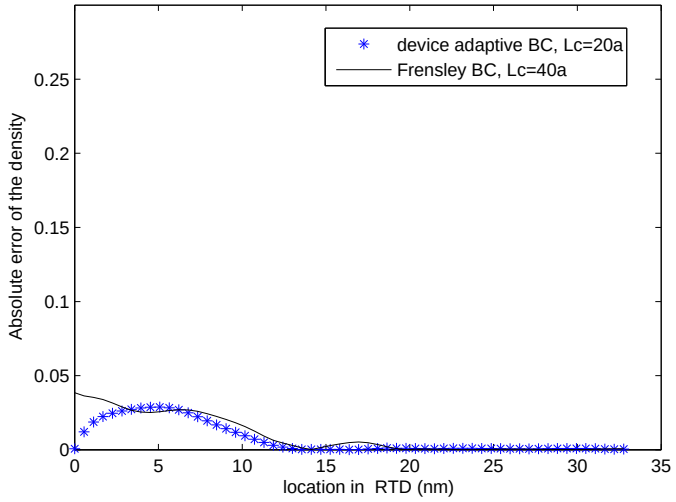

Fig. 14. The absolute error of the density with the two inflow boundary conditions and different lengths of the contacts

the DABC with $L_c = 20a$ is close to that of the Frensley boundary condition with $L_c = 40a$. To make it more clearly, taking the density of the Frensley inflow boundary condition with $L_c = 40a$ as the reference solution, we get the relative errors of the density of the two inflow boundary conditions with $L_c = 20a$ in the left sub-figure of Fig. 15. It shows that for a given accuracy, the DABC allows to use a much shorter contact length, thus much smaller computational domain than the Frensley inflow boundary condition. So the DABC is a more efficient domain truncation method for simulating nano-scale devices in open systems.

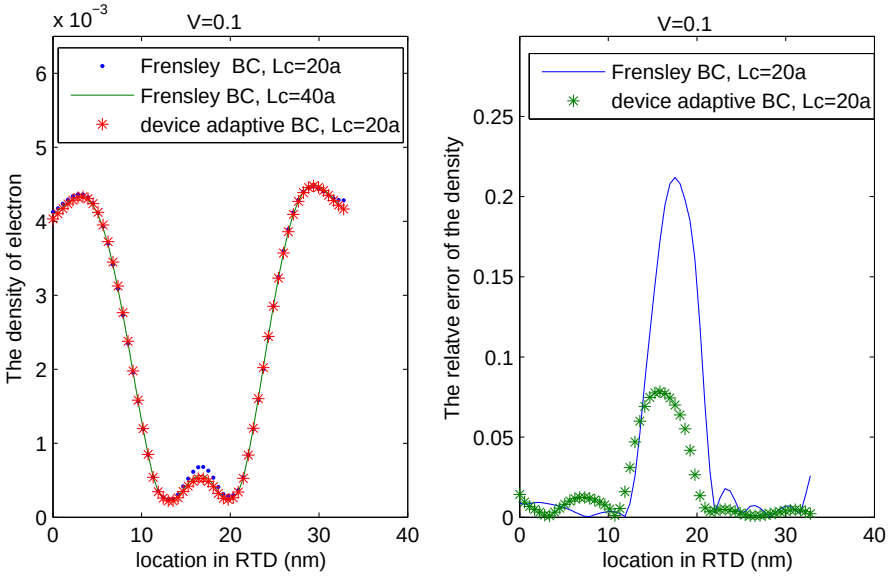

Fig. 15. The results of multi-injection with the two inflow boundary conditions

6. Conclusion and future work

In this paper, we proposed a device adaptive boundary condition (DABC) of inflow type for the Wigner equation in quantum transport. This new boundary condition considers the global nature of the Wigner functions and includes the effect of the device internal band structure on the behavior of the electrons in the contacts. The conventional application of the Frensley inflow boundary condition uses a boundary value based on the semi-classical Fermi-Dirac distribution, which does not include the quantum interaction due to the internal band structure of the device. The DABC corrects this situation by setting the boundary value of the Wigner function to be that of the Wigner function based on the wave function of the quantum device at zero bias. This approach allows the inclusion of the dominant quantum behavior due to the device band structure into the physical picture of the electrons in the contacts. Numerical tests on resonant tunneling diodes at a wide range of non-zero biases show significant improvement in the electron density calculation with the new boundary condition and also the reduction of the contact length to be included in the simulation, reducing the overall computational cost for a given desired accuracy.

Further research is underway to study how the boundary value for the Wigner function can be found for more general quantum devices beyond the 1-D RTDs considered here and apply the DABC to the self-consistent Poisson-Wigner equations, where nonlinear effects in the one-particle electron model in the Poisson-Wigner equations will be addressed, and also investigate the effect of DABC on the computation of the I-V characteristic of the RTDs and nanoscale MOSFETs.

Acknowledgments

Authors thank for the support of Army Research office (Grant No. W911NF-07-1-0492) and NSFC Grant (No.10828101). H. Y. Jiang is also supported by NSFC Grant(61072097, 91230107) and NSFC Tian Yuan Young Scholars Grant (10726025). T. Lu is also supported by NSFC Grant (11011130029, 91230107).

References

[1] S. Datta. *Quantum Transport: Atom to Transistor.* Cambridge Univ. Press, Cambridge, U.K, 2005.

[2] W. Cai. *Computational Methods for Electromagnetic Phenomena: Electrostatics in Solvation, Scattering, and Electron Transport*. Cambridge Univ. Press, Cambridge, U.K, 2013.

[3] H. Jiang, S. Shao, W. Cai, and P. Zhang. Bounadry treatment in non-equilibrium Green's function(NEGF) methods for quantum transport in nano-MOSFETs. *J. Comput. Phys.*, 227:6553–6573, 2008.

[4] H. Jiang and W. Cai. Effect of boundary treatments on quantum transport current in the Green's function and Wigner distribution methods for a nano-scale DG-MOSFET. *J. Comput. Phys.*, 229(12):4461–4475, 2010.

[5] S. Datta. Nanoscale device modeling: the Green's function method. *Superlattices and Microstructures*, 28:253–278, 2000.

[6] R. Venugopal, Z. Ren, S. Datta, M. S. Lundstrom, and D. Jovanovic. Simulating quantum transport in nanoscale transistors: Real versus mode-space approaches. *J. Appl. Phys.*, 92:3730–3739, 2002.

[7] Z. Ren, R. Venugopal, S. Goasguen, S. Datta, and M. S. Lundstrom. nanoMOS 2.5: A two-dimensional simulator for quantum transport in double-gate MOSFETs. *IEEE Trans. Electron Devices*, 50(9):1914–1924, 2003.

[8] E. Wigner. On the quantum correction for thermodynamic equilibrium. *Phys. Rev.*, 40(5):749–759, Jun 1932.

[9] P.A. Markowich, C.A. Ringhofer, and C. Schmeiser. *Semiconductor Equations*. Springer, Vienna, 1990.

[10] M. Nedjalkov, D. Querlioz, P. Dollfus, and H. Kosina. Wigner function approach. In D. Vasileska and S.M. Goodnick, editors, *Nano-Electronic Devices: Semiclassical and Quantum Transport Modeling*. Springer, New York, 2011.

[11] W.R. Frensley. Wigner function model of a resonant-tunneling semiconductor device. *Phys. Rev. B*, 36:1570–1580, 1987.

[12] P.J. Zhao and D. Woolard. Wigner-Poisson model based nano-electronic engineering modeling and design. *Dynamics of continuous, discrete & impulsive systems, Series B, Applications & algorithms*, 2:854–859, 2005.

[13] H. Tsuchiya and M. Ogawa. Simulation of quantum transport in quantum device with spatially varying effective mass. *IEEE Trans. Electron Devices*, 38(6):1246–1252, 1991.

[14] S. Shao, T. Lu, and W. Cai. Adaptive conservative cell average spectral element methods for transient Wigner equation in quantum transport. *Commun. Comput. Phys.*, 9:711–739, 2011.

[15] J.J. Shih, H.C. Hunag, and G.Y. Wu. Effect of mass discontinuity in the Wigner theory of resonant-tunneling diodes. *Phys. Rev. B*, 50(4):2399–2405, 1994.

[16] L. Shifren, C. Ringhofer, and D.K. Ferry. A Wigner function-based quantum ensemble Monte Carlo study of a resonant tunneling diode. *IEEE Trans. Electron Devices*, 50:769–773, 2003.

[17] D. Querlioz, P. Dollfus, V. N. Do, A. Bournel, and V. L. Nguyen. An improved Wigner Monte-Carlo technique for the self-consistent simulation of RTDs. *J. Comput. Electron*, 5:443–446, 2006.

[18] H. Kosina and M. Nedjalkov. Wigner function-based device modeling. In M. Rieth and W. Schommers, editors, *Nanodevice Modeling and Nanoelectronics*, volume 10 of *Handbook of Theoretical and Computational Nanotechnology*. American Scientific Publishers, 2006.

[19] V. Sverdlov, A. Gehring, H. Kosina, and S. Selberherr. Quantum tranport in ultra-scaled double-gate MOSFETs: A Wigner function-based Monte Carlo approach. *Solid State Electronics*, 49:1510–1514, 2005.

[20] A. Gehring and H. Kosina. Wigner function-based simulation of quantum transport in scaled DG-MOSFETs using a Monte Carlo method. *J. Comput. Electr.*, 4:67–70, 2005.

[21] G.A. Kathawala, B. Winstead, and U. Ravaiolo. Monte Carlo simulations of doulbe-gate MOSFETs. *IEEE Trans. Electronic Devices*, 50(12):2467–2473, 2003.

[22] D. Querlioz, J. Saint-Martin, V.-N. Do, A. Bournel, and P. Dollfus. A study of quantum transport in end-of-roadmap DG-MOSFETs using a fully self-consistent Wigner Monte Carlo approach. *Nanotechnology, IEEE Transactions on*, 5(6):737–744, Nov. 2006.

[23] K. L. Jensen and F. A. Buot. Numerical simulation of intrinsic bistability and high-frequency current oscillations in resonant tunneling structures. *Phys. Rev. Lett.*, 66:1078–1081, Feb 1991.

[24] P.J. Zhao, D.L. Woolard, and H.L. Cui. Multisubband theory for the origination of intrinsic oscillations within double-barrier quantum well systems. *Phys. Rev. B*, 67:085312, Feb 2003.

[25] H. Jiang, W. Cai, and R. Tsu. Accuracy of the frensley inflow boundary condition for wigner equations in simulating resonant tunneling diodes. *J. Comput. Phys.*, 230:2031–2044, 2011.

[26] C. Jacoboni, R. Brunetti, P. Bordone, and A. Bertoni. Quantum transport and its simulation with the Wigner function approach. *Int. J. High Speed Electron. Syst.*, 11:387–423, 2001.

[27] C. Jacoboni and P. Bordone. The Wigner-function approach to non-equilibrium electron transport. *Rep. Prog. Phys.*, 67:1033–1071, 2004.

[28] M. Hillery, R.F. ÓConnell, M.O. Scully, and E.P. Wigner. Distribution functions in physics: Fundamentals. *Physics Reports*, 106(3):121–167, 1984.

[29] D. K. Ferry and S. M. Goodnick. *Transport in Nanostructures*. Cambridge Univ. Press, Cambridge, U.K, 1997.